Research Square

Preprints are preliminary reports that have not undergone peer review.
They should not be considered conclusive, used to inform clinical practice,
or referenced by the media as validated information.

A survey of plankton and anthropogenic particles across the tropical and subtropical North Atlantic

Howard Dryden

drydenaqua@me.com

Goes Foundation

Diane Duncan

Goes Foundation

Research Article

Keywords: near-surface ocean, microplastics, anthropogenic particles, zooplankton, North Atlantic, citizen science, sailing yachts, surface microlayer

Posted Date: November 26th, 2026

DOI: https://doi.org/10.21203/rs.3.rs-11729098/v1

License: This work is licensed under a Creative Commons Attribution 4.0 International License.
Read Full License

Additional Declarations: The authors declare potential competing interests as follows: The authors are associated with the GOES Foundation, a not-for-profit organisation originally based on the sailing vessel Copepod and now located at www.seahorsepoint.org in Bocas del Toro, Panama, and H.D. designed the GOES filter that this paper evaluates. The authors declare that they have no financial competing interests.

Abstract

Few surveys sample the top metre of the open ocean, and to our knowledge none has counted plankton and anthropogenic particles together along an east-to-west crossing of the tropical and subtropical North Atlantic. Thirteen sailing yachts filtered half-litre samples of near-surface seawater between the Canary Islands, Cape Verde and the Caribbean from December 2021 to February 2022. Image analysis sized and classified 18,142 particles larger than 20 micrometres in 1,466 microscope photographs, which represent 146.6 litres of seawater. Dark opaque particles were the most abundant class at about 64,000 particles m^{-3}, and suspected microplastic fibres and particles together reached about 6,400 m^{-3}. Almost all particles were smaller than 250 micrometres, and five large zooplankton were found, a density of 34 individuals m^{-3} with a 95% interval of 11 to 80. We conclude that, in this size range, anthropogenic particles far outnumber plankton on this crossing and that microzooplankton were absent.

Introduction

Most of what we know about plankton and particles in the open ocean comes from research vessels, which sample mainly between 5 and 200 m depth and rarely resolve particles smaller than the mesh of a plankton net, which is typically 200 to 330 µm[1,2]. Cruising sailing yachts cross oceans that research vessels seldom visit, on tracks and at times that no programme funds. A small crew can sample from a yacht without winches, wire, laboratory space or power. This makes yachts a practical platform for volunteer sampling when the sampler is simple enough for every crew to use in the same way.

We use three depth terms throughout this paper: the surface microlayer is the film at the air–sea interface that is less than 1 mm thick; the near-surface layer is the top metre, of which this survey sampled the upper 250 mm; and the epipelagic layer is the water from the surface down to 200 m. The sampler fills by immersion, so it collects a bulk sample of near-surface water and does not separate the microlayer.

The near-surface layer is worth sampling directly, because the two polymers made in the largest volumes, polyethylene and polypropylene, are less dense than seawater and float[3,4], and together they dominate the polymers recovered at the sea surface[5]. Buoyant plastic concentrates in the top few centimetres and falls away with depth as biofouling adds density and wind mixing carries particles down[6,7]. Sampling below the surface, or through a coarse net, therefore misses much of this material. The standing stock of the smallest surface plankton and the burden of anthropogenic particles of 20 to 250 µm are also poorly known.

The trade-wind tropical and subtropical North Atlantic is an oligotrophic region that is influenced by the subtropical gyre and crossed by the North Equatorial and Canary currents, where surface productivity is expected to be low. Saharan dust supplies iron, while nitrogen and phosphorus limit growth, and iron and phosphorus together limit nitrogen fixation in the eastern part of the region[8,9,10]. We therefore expected few mesozooplankton but some microzooplankton, such as copepod nauplii and early copepodites of 20

to 200 µm. The region also contains the Main Development Region, the corridor in which most major Atlantic hurricanes form[11]. Research vessels have crossed this corridor, but to our knowledge none has surveyed the plankton and particles of the top metre along its length from Africa to the Caribbean, and the organisms that build and break down the surface microlayer here have not been sampled.

The surface microlayer regulates the exchange of gases between ocean and atmosphere and supplies the aerosols that seed marine clouds[12]. The oceans supply 86% of global evaporation[13], and surfactant films have been measured to reduce the air–sea transfer velocity of carbon dioxide by up to 32% in the Atlantic[14] and by up to 62% inside slicks[15], while cyanobacterial surface blooms have been observed to inhibit evaporation from the skin layer[16], which indicates that the same film can also slow the escape of water vapour. The trade-wind Atlantic is also where much of the energy that warms high latitudes leaves the sea, because the atmosphere carries latent heat in water vapour and sensible heat in dry air from the tropics towards the Arctic, and at 35° N it carries 78% of the total poleward heat transport of the Northern Hemisphere, while the ocean carries 22%[17]. The atmospheric transport peaks at 5.0 PW near 43° N, about four times the 1.3 PW that the Atlantic overturning circulation, including the Gulf Stream, carries across 26.5° N[17,18]. These roles are a reason to know which particles and organisms occur near the interface where evaporation takes place.

We asked what the near-surface layer holds: how many plankton and how many anthropogenic particles it contains and at what sizes. Behind that measurement sits a larger question: whether the biological regulation of what we consider the most climatically significant surface on Earth, an interface covering about 71% of the planet and central to a range of global biogeochemical and climate-related processes[19], is being disrupted by anthropogenic particle pollution in ways that current models do not represent. In our view this is one of the more important unasked questions for Earth system modelling, and the answer depends on data from the ocean surface, which this survey begins to supply. We report 1,466 photographs from thirteen yachts, and the results are a first baseline for the near-surface layer of this region.

Results

Survey coverage and sample set

Thirteen sailing yachts contributed counted photographs, and they sampled the zonal trade-wind corridor from the Canary Islands and Cape Verde to the Caribbean and Suriname between 18 December 2021 and 11 February 2022 (Fig. 1). One yacht, Emma, also sailed a higher-latitude return leg from west to east between 19 May and 31 July 2022, which is the only part of the archive outside the trade-wind belt and the winter season. Crews filled the GOES sampler (Fig. 2) at about 12-hour intervals, at local noon and midnight, and photographed each filter under a digital microscope (Methods).

The analysis uses 1,466 photographs of the trade-wind crossing, which represent 146.6 litres of filtered seawater, of which 118.7 litres fall inside the counted area. The 271 photographs of the return leg

represent 27.1 litres filtered and 22.0 litres counted. Supplementary Table S1 lists the photographs and counted litres of each vessel.

Particle classes and concentrations

The image pipeline sized and classified 18,142 objects in the 1,466 accepted photographs. Dark opaque particles were present in 70.2% of photographs (6,671 objects), mineral grains in 57.2%, plant debris in 54.9%, unidentified objects in 51.0%, suspected microplastic fibres in 26.7%, phytoplankton in 24.1% and suspected microplastic particles in 3.1% (Table 1). Suspected microplastics are objects that look like plastic by colour and shape, and chemical confirmation by spectroscopy is planned for the next campaign. The class names microplastic fibres and microplastic particles are used in that sense throughout the paper.

Table 1
Summary of the particle and plankton classes on the two legs of the survey. The trade wind crossing is the east-to-west passage of thirteen yachts from the Canary Islands and Cape Verde to the Caribbean between December 2021 and February 2022 (1,466 photographs, 146.6 litres filtered, 118.7 litres counted). The return leg is the west-to-east passage of the yacht Emma at higher latitude in May to July 2022 (271 photographs, 27.1 litres filtered, 22.0 litres counted). For each class the table gives the share of photographs in which the class was present, the mean concentration in particles per cubic metre of counted volume after correction for the error rates of the blind eye check, and the number of objects counted, and the zooplankton densities are calculated on the volume filtered. All classes except the zooplankton are optical classes assigned by the image pipeline and await confirmation by spectroscopy, and the unidentified class corrects to zero because it resolves mainly to dark opaque particles. The uncorrected concentrations, the 95% Wilson intervals and the fibre lengths are given in Supplementary Table S3.

Class	Crossing: share of photographs	Crossing: particles m^{-3}	Crossing: objects counted	Return leg: share of photographs	Return leg: particles m^{-3}	Return leg: objects counted
Zooplankton	0.2%	34	5	0%	0	0
Microzooplankton (radiolarians)	0%	0	0	5.5%	800	18
Phytoplankton	24.1%	9,000	695	7.0%	3,600	22
Dark opaque particles	70.2%	64,200	6,671	68.3%	24,600	473
Microplastic particles	3.1%	1,400	65	2.6%	700	7
Microplastic fibres	26.7%	5,000	782	16.6%	1,900	62
Mineral grains	57.2%	24,100	3,881	28.0%	5,400	109
Plant debris	54.9%	28,000	4,233	54.6%	10,700	342
Unidentified	51.0%	0	1,815	42.1%	0	196

Particle counts are strongly right-skewed, and most photographs hold zero or one object of a given class, so each class is summarised by its mean across the archive. After correction for the error rates measured in the blind eye check, the means for the trade-wind crossing are 64,200 m⁻³ for dark opaque particles, 28,000 m⁻³ for plant debris, 24,100 m⁻³ for mineral grains, 9,000 m⁻³ for phytoplankton, 5,000 m⁻³ for microplastic fibres and 1,400 m⁻³ for microplastic particles. The correction also removed 21,100 m⁻³ of stains and rejected objects from the totals. Photographs along one track sample similar water, so we treat each vessel as one independent sample, and the thirteen vessels give thirteen replicate estimates of each concentration. Dark opaque particles, plant debris, mineral grains and suspected microplastic fibres were recorded by all thirteen vessels, so the presence of these classes does not depend on any one vessel. The standard deviations of the thirteen vessel means before correction were 63,000 m⁻³ for dark opaque particles, 31,000 m⁻³ for plant debris, 30,000 m⁻³ for mineral grains and 4,500 m⁻³ for microplastic fibres (Supplementary Table S1). These values show how much concentrations varied from vessel to vessel, and the Wilson intervals in Supplementary Table S3 give the counting precision within the archive. Copepod, the vessel sailed by the authors, recorded the highest mean for dark opaque particles (248,900 m⁻³ before correction), and without that vessel the mean for the crossing before correction falls from 56,200 to 45,200 m⁻³.

On the return leg, the seven optical classes assigned by the pipeline total 46,900 m⁻³ after correction, compared with 131,700 m⁻³ on the trade-wind crossing, a ratio of 2.8 (Table 1), and the radiolarians found by eye on the return leg add a further 800 m⁻³. Emma sailed both legs, and its own crossing photographs give 156,400 m⁻³ before correction against 55,200 m⁻³ on its return leg, the same ratio of 2.8 on a single vessel (Supplementary Tables S1 and S3). Three representative filter fields, each from a different station, show the range of material: a blue copepod, a long blue microplastic fibre with a black fibre coil, and brown mineral grains with dark opaque particles (Fig. 3).

Particle sizes

Of all classified objects, 99.99% measured below 250 µm and 99.6% measured below 100 µm, clustered just above the nominal 20 µm limit of filtration and imaging (Fig. 4a). Power-law exponents fitted over 20 to 100 µm, where the counts are robust, were − 3.6 (95% confidence interval − 4.1 to − 3.2) for dark opaque particles, − 3.6 (− 4.5 to − 2.8) for plant debris and − 2.8 (− 3.3 to − 2.3) for mineral grains, with $p < 0.0001$ for each. Microplastic fibres were nearly flat at − 0.5 (− 0.9 to 0.0, $p = 0.048$) and formed a distinct larger mode, which reached an equivalent diameter of 254 µm in the single largest case, a fibre 2.3 mm long. Phytoplankton rose with size at + 0.8 (+ 0.1 to + 1.6, $p = 0.038$), as expected for cells and colonies rather than fragments. Microplastic particles gave − 1.1 (− 2.1 to − 0.2, $p = 0.026$), an estimate from 65 objects. These class shapes were not built into the classifier, so their agreement with the expected behaviour of each material gives independent support for the classification. These counts cover particles of 20 µm and above, so they are a conservative measure of the total particle burden, which also includes smaller particles.

Distribution along the crossing from east to west

We tested for an east-to-west gradient in every class (Fig. 5a). The class means show no strong longitudinal gradient, and no fitted slope is significant at the 5% level. The steepest slopes were for dark opaque particles ($p = 0.07$) and microplastic fibres ($p = 0.08$), and both fall towards the west. Three weak per-photograph rank correlations reached nominal significance, with Spearman coefficients of − 0.22 for dark opaque particles, − 0.15 for microplastic fibres and − 0.07 for unidentified objects. Photographs along one track sample similar water, so we rest the conclusion on the binned fits, which are the more conservative test. Thirteen vessels are enough to detect a gradient larger than the scatter between vessels, and none was found. More vessels will resolve any weaker spatial structure, and the return leg is shown in Fig. 5b.

Animals in the filter samples

Every object of 250 µm and above in the archive was checked by eye. This confirmed five animals: two blue copepods of about 1,600 µm on the filter discs of counted photographs and three decapods of about 7 mm to above 20 mm that came from the 0.5-litre samples but lay outside the counted disc after handling. The copepods were found by the yachts Misty Blue (22 January 2022, 15.48° N, 32.60° W, by day) and Emma (6 February 2022, 11.91° N, 40.73° W, at night). The decapods were found by Eleuthera (26 January 2022, 13.68° N, 42.38° W, by day, two shrimps of about 14 mm and above 20 mm) and by Misty Blue (5 February 2022, 12.08° N, 60.88° W, after dark, one shrimp of about 7 mm). On the 146.6 litres filtered, five animals give a density of 34 individuals m^{-3}, with an exact 95% Poisson interval of 11 to 80 individuals m^{-3}.

We searched the crossing for microzooplankton with a dedicated class in the classification and inspected 776 candidate objects by eye at full resolution. Of these, 585 were compact particles, 191 were elongated filaments, and none was an animal, so microzooplankton were absent from the crossing. On the return leg, 18 radiolarians of about 20 to 60 µm were identified in the 22.0 counted litres, which is about 800 individuals m^{-3} and lies within the range of 1 to 5,000 individuals m^{-3} reported for radiolarians in the upper 1,000 m of the world's oceans[21,22]. The counted photographs of the return leg held no animal zooplankton, and a zero in 22 litres is consistent with the median of 1.1 copepods m^{-3} recorded at thirteen stations between 25° N and 35° N in the Tara Pacific crossing[2,23].

Accuracy of the classification

We tested the classification with three blind marking sheets that the lead author scored with the machine class hidden (Methods). A second scorer then rescored all 780 marked objects blind. Twelve objects lacked a verdict from one scorer, which left 768 pairs. The two scorers agreed on 65.4% of objects across seven classes (Cohen's kappa 0.577), with kappa between 0.545 and 0.599 across the four marking documents. Agreement rose to 78.5% (kappa 0.648) when the classes were collapsed into anthropogenic, natural and other groups (Supplementary Table S2). Most differences between the

scorers lay among visually similar pale particles, and the second scorer assigned 18 objects to the phytoplankton class against 53 by the first scorer, so the phytoplankton concentration is an upper estimate. An independent detection pass reproduces the total particle load within about 10%, so the total is robust to the classification rules, which affect the split between plastic-like, dark and unidentified objects.

We therefore grade the confidence of the results: it is high for particle detection, approximate size, total abundance and the presence of the broad optical categories, and moderate for the blue microplastic fibres and for the large objects confirmed by eye. Phytoplankton, the chemical identity of the dark opaque class, the separation of mineral grains from plant debris, and the non-blue microplastics are provisional at this stage, and the spectroscopy planned for the next campaign will test the particle classes. Blue is the colour that we identify as plastic-like with confidence, so the microplastic count is most secure for blue items and is conservative.

Comparison with a satellite dust budget

Mineral grains allow a check against an independent measurement: the survey counted 32,700 grains m^{-3} by machine, at a median diameter of 30 µm. Treated as plates with three tenths of the volume of a sphere of the same optical diameter and summed grain by grain, the 3,881 grains give 0.73 mg m^{-3}. Scaling by the eye-corrected count of 24,100 grains m^{-3} gives about 0.54 mg m^{-3}. A satellite-based dust budget of about 139 million tonnes per year over 21.2 million km^2 predicts 0.84 mg m^{-3} for slowly settling plates[24,25]. The measured load is therefore within 13% of the prediction and the corrected load is within 36%, both on the low side. Grain shape enters both sides of the comparison, so the agreement is a consistency check.

Satellite view of the study region

Satellite chlorophyll-a for January and February 2022 places the crossing in oligotrophic water on the southern flank of the subtropical gyre (Fig. 6). The median over the transect box was 0.11 mg m^{-3}, and 86% of the box lay below an operational oligotrophic threshold of 0.15 mg m^{-3}. The January to February median for 2012 to 2021 was 0.12 mg m^{-3}, so the pattern is climatologically stable. Elevated chlorophyll was confined to the Mauritanian and equatorial upwellings and to the continental margins. Over the wider north tropical Atlantic, annual mean chlorophyll-a showed no trend from 1998 to 2025 ($p = 0.98$), while the diffuse attenuation coefficient Kd490 rose by about 5 to 6% from 2003 to 2021 ($p = 0.04$ on the merged record, Supplementary Fig. S1). Over those same years chlorophyll-a also rose, by about 7%, but not significantly ($p = 0.47$), and attenuation rose faster than the year-to-year relation between the two predicts ($p = 0.03$). Kd490 is computed from the same blue-green reflectance ratio as chlorophyll-a, and dissolved coloured organic matter also raises it, so this excess points to an increased load of non-algal particles or dissolved colour, and separating the two needs samples from the water itself. An independent 28-year record from SeaWiFS, MODIS-Aqua and VIIRS gives the same picture, because

chlorophyll-a averaged over the permanently stratified ocean between 40° S and 40° N held at 0.136 mg m^{-3} from 1997 to 2025 with a standard deviation of 5.7%, and no long-term trend is reported[26].

Colour change of this kind is widespread, because 20 years of MODIS reflectance show significant trends over 56% of the global surface ocean, mostly equatorward of 40°[27]. Several causes are possible, because a change in plankton community structure toward smaller cells, a change in detritus or dissolved colour, and an increased load of suspended particles each alter reflectance without a matching change in chlorophyll, so satellite data need direct sampling to separate them[27,28]. A model of the warming and more stratified ocean predicts the shift toward smaller cells and shows that it changes reflectance before it changes chlorophyll[28], and the 28-year satellite record already shows chlorophyll-a and phytoplankton carbon diverging in places, which is the signature of a change in community composition or physiology rather than in biomass[26]. The same nutrient stress drives the release of exopolymers, which raise the microscale viscosity of the water[29] and aggregate into transparent particles that scatter light without adding chlorophyll[30], so a shift to smaller cells and a rise in non-algal particles are expected together. Such optical change is now being sought from space: three 20-year satellite records, including the same OC-CCI product used here, show a progressive brightening of blue and green reflectance around the Great Pacific Garbage Patch between 2002 and 2022, and radiative transfer modelling makes that colour shift more than four times as likely when suspended microplastics are included, although the authors state that the pattern alone does not prove the cause[31].

Discussion

To our knowledge, no previous survey has sampled the trade-wind crossing of the tropical and subtropical North Atlantic for near-surface plankton and anthropogenic particles together, so this survey gives the first baseline for the region at 20 µm resolution, against which later surveys can measure change.

Almost all particles were smaller than 100 µm, a size range that plankton nets with meshes of 200 to 330 µm do not retain. Counts from this method and from nets therefore describe different fractions of the same water. The Tara Pacific comparison shows the same point, because the 18 radiolarians of the return leg lie in a fraction that the 330 µm mesh of that survey cannot retain[2,23]. The near-surface fraction also sits on a large subsurface stock, because Pabortsava and Lampitt found 11.6 to 21.1 million tonnes of polyethylene, polypropylene and polystyrene of 32 to 651 µm suspended in the top 200 m of the Atlantic[32], and the fibres and particles we counted, about 6,400 m^{-3} at 20 to 250 µm, are the near-surface expression of that stock. Their pump samples at 10 m held 990 to 6,999 particles m^{-3} of the three polymers combined, a range that contains our count, and the highest subsurface values in the northern gyre were at 15° N near Cape Verde, where our transect begins[32]. Below our 20 µm floor the burden continues, because nanoplastics smaller than 1 µm, which lie below the resolution of light microscopy, amount to about 27 million tonnes in the mixed layer of the temperate and subtropical North Atlantic[33]. Above it, the surface microlayer concentrates microplastics relative to the water beneath, and

glass-plate samples of the microlayer in a British estuary were more than 99% fibres, three quarters of them black, with polyethylene the most common polymer identified[34]. Identification in this survey is optical, which allows particles in this size range to be counted in large numbers, and the blind check gives each class a measured error rate. Visual sorting is known to differ from spectroscopy for a share of microplastics[35], and sampling methods for microplastics in water differ in how they quantify particles[36], so we report the optical classes with their measured error rates. Optical classes with known error rates, replicated across many places and times, can describe the distribution, abundance and trend of particle classes in the near-surface layer, and the chemical identity of single particles will follow from spectroscopy of the sealed filters planned for the next campaign. Suspected microplastic fibres were recorded by all thirteen vessels, far from land sources and with no strong east-to-west gradient, which is consistent with wet and dry atmospheric deposition as a pathway[37,38]. Saharan dust along this route is deposited mainly dry in winter[39], so dry deposition is the more likely of the two during the survey months.

Dark opaque particles dominated the anthropogenic load, and they are far larger than soot, because an aged soot aggregate measured at a remote North Atlantic site is 0.21 to 0.28 µm across[40], a hundred times below the 20 µm floor of this method. Angular dark particles would be consistent with char, the solid residue of burning, which is reported at 1 to 100 µm with axis ratios of 1.5 to 2.4[41,42], and round ones with the spheroidal carbonaceous particles that coal and heavy fuel oil produce above 1,000 °C[43]. Tyre and road wear is a leading candidate because its number-median diameter of 34 µm lies inside the size range of the dark opaque particles recorded here[44]. Two questions about transport follow from this candidate: modelled long-range transport covers particles of 0.5 to 10 µm[45], and tyre particles are denser than seawater, with settling velocities of 0.2 to 0.7 mm s^{-1}[46], so their presence in the top metre would point to a continuous supply from above. Coal dust, bitumen, brake wear and dark volcanic glass also appear as black angular objects of the same size under transmitted light[44,47]. We therefore keep all of these candidates open, and the spectroscopy planned for the next campaign is designed to identify the source.

Whatever their source, any combustion carbon among the dark opaque particles matters for chemical pollution, because black carbon is among the strongest environmental sorbents of hydrophobic organic contaminants and binds them one to two orders of magnitude more strongly than amorphous organic matter[48]. Plastic resin pellets from coastal waters carry persistent organic pollutants such as PCBs and DDE at up to about a million times the concentrations in the surrounding seawater[49], and partially combusted carbon sorbs the same compounds more strongly still[50], so where the plastic vector for such chemicals is modest relative to other pathways[51], black carbon is the stronger carrier in the same water and goes almost entirely unmeasured.

These persistent organic pollutants reach the sea because conventional wastewater treatment does not destroy them: the hydrophobic compounds are removed from the water only by sorption to the sludge, with 65 to 91% removal for individual PCBs and pesticides at a municipal plant, with the remainder

passing in the effluent[52], while the perfluorinated compounds pass secondary treatment almost unchanged and are often more concentrated in the effluent than in the raw sewage[53]. Sewage sludge containing these persistent organic pollutants is often disposed of by application to agricultural land[54,55]. These chemicals can therefore return in food, food waste and agricultural run-off[56,57]. Far from land, legacy pollutants such as PCBs reach the ocean mainly by atmospheric transport and deposition[58,59]. Once at sea the same hydrophobic compounds float in the surface microlayer, where chlorinated hydrocarbons, petroleum hydrocarbons and polycyclic aromatic hydrocarbons are enriched by up to 500 times relative to the water beneath[60], in the same layer that holds the buoyant plastic and the particles counted here. Both particle classes can carry these chemicals into the base of the food web[48,61], and polystyrene microplastics carrying sorbed triclosan were an order of magnitude more toxic to human intestinal cells than the same particles clean[62]. The surface microlayer supplies the organic fraction of the marine aerosol that seeds clouds[63], and airborne microplastic is deposited in rain far from its sources[37,38], so particles of plastic and carbon, and the chemicals bound to them, can be redistributed in rainfall around the globe.

A circumglobal survey of tropical and subtropical stations found no significant difference in zooplankton among ocean basins, with depth the dominant factor and the highest values near upwelling areas[1]. Its depth-integrated daytime abundance in the upper 200 m was usually above 200 individuals m^{-3} on a 300 μm mesh[1]. The productivity maximum of oligotrophic water lies at the deep chlorophyll maximum, which in the Atlantic subtropical gyres occupies a layer from about 67 to 126 m and is a permanent feature of tropical and subtropical waters[64,65], so zooplankton that feed on phytoplankton are likely to be most abundant there, well below the layer that we sampled. Mesozooplankton were present, because the five animals give 34 individuals m^{-3}, but microzooplankton were absent from the crossing. Visual predation and high ultraviolet exposure in clear water are plausible reasons for a genuine near-surface scarcity of microzooplankton[66,67,68]. A further hypothesis, which a later campaign could test, is that the ferric iron supplied by Saharan dust changes the physical state of the water: hydrolysed iron destabilises colloids by lowering their surface charge and promotes coagulation[69], dust deposition triggers the formation of transparent exopolymer particles[70], and such exopolymers raise the viscosity of seawater at the scale of small organisms[29,71], which slows the swimming and feeding of small plankton[72] while leaving larger animals less affected. The same dust-driven coagulation and exopolymer formation would add non-algal particles that raise light attenuation without adding chlorophyll, which matches the sign of the Kd490 rise in Supplementary Fig. S1. No trend in dust supply is recorded over the same period, so a rising attenuation would require a rising driver elsewhere in the chain, and the exopolymer release that stratification and nutrient stress promote is the one candidate with a documented trend. The same iron acts on the particles, because trace iron catalyses photo-Fenton reactions that accelerate the oxidative ageing of plastic surfaces[73]. Toxic loading is known to affect grazing zooplankton elsewhere[74,75], and we note it as a candidate mechanism, because our survey records the absence of microzooplankton alongside many anthropogenic particles, and the cause is a question for targeted experiments. Other

candidates, including nutrient stripping by the Great Atlantic *Sargassum* Belt, are outlined in Supplementary Note 1 as hypotheses for future work.

The harm that plastic does to the organisms of the near-surface layer is well established in the laboratory, because polystyrene microplastics reduce feeding and reproductive output in the copepod *Calanus helgolandicus*[76], polystyrene particles reduce the growth of the microalga *Dunaliella tertiolecta*[77], and leachates from common plastics impair the growth and photosynthesis of *Prochlorococcus*, the most abundant photosynthetic organism in the ocean[78]. Those exposures used far higher concentrations than occur at sea, and Cole and colleagues dosed copepods at 75 beads per millilitre, about ten thousand times the 6,400 m^{-3} of suspected microplastics counted here[76]. Both particle studies also used smooth spheres, whereas plastic at sea breaks into irregular fragments, and polyethylene fragments of about 37 µm, within the size range counted here, were more than 80 times more acutely toxic to the freshwater crustacean *Daphnia magna* than beads of the same size, probably because of their irregular shape and larger specific surface area[79,80]. They also used new plastic, and weathering makes the problem worse, because ageing at sea roughens and oxidises the particle surface, shifts its surface charge and raises its adsorption of metals, organic pollutants and antibiotics[73], and ultraviolet exposure and ageing increase the toxicity of plastic leachates to copepods[81] and to microalgae[82], so the laboratory results are conservative for plastic that has aged in the ocean. Our count also stops at 20 µm, and the smaller micro- and nanoplastics, of which the mixed layer of the temperate and subtropical North Atlantic holds about 27 million tonnes of nanoplastic alone[33], present a far larger surface area per unit mass for sorbed contaminants and for contact with cells, because surface area per unit mass rises as particle size falls. The harm extends up the food web, because nano- and microplastics damage the gut, gills, liver and nervous system of marine and freshwater fish, and up to 80% of captured marine fish have been reported to contain microplastics[83]. Phytoplankton and zooplankton produce the oils and surfactants that form the surface microlayer[84,85,86], so if microplastics and persistent organic pollutants affect the plankton, they affect the microlayer and may in turn affect the weather. Suspected microplastics were present in more than a quarter of our photographs, so the near-surface community of this region lives with a stressor that is known to harm plankton from copepods to cyanobacteria. Whether the condition of the microlayer measurably changes the rate of ocean evaporation is an open and testable question. A quantitative test would need paired eddy-covariance measurements of latent heat flux inside and outside natural slicks, set against measured surfactant cover.

The strength of the method is coverage, because thirteen vessels sampling twice a day gave 1,466 photographs along a track that research vessels seldom visit, and more vessels or more frequent sampling will add the filtered volume needed to compare the biomass of sparse plankton in oligotrophic water. A volunteer survey complements a research cruise, because a large number of observations over a wide area can give a more informative picture than a small number of highly precise measurements.

The first lesson of the survey is to keep the samples, so in the next campaign a subset of filters will be dried and sealed in airtight containers after the preservation method has itself been tested so that dark and plastic-like particles can be checked by FTIR or Raman spectroscopy on land. Sampling will rise to four times daily to strengthen the rarer classes and to give the plankton the volume it needs. Simple screening methods, such as Nile Red staining of microplastics, could be tested as a way to strengthen identification without losing accessibility. The key requirement is a sharp, in-focus image from a microscope of at least 5 megapixels with a polarising filter, and better training in focusing the microscope and fitting the polarising filter would raise the yield of usable photographs. The sampler is not restricted to ocean-going vessels, so samples could also be collected from rivers, lakes, piers, the coast, small coastal boats and rainwater, and a standardised dataset could then link particles from land and sky to the ocean. Ten thousand samplers in use around the world, each photographed to the same protocol, would yield a global record of near-surface particles and plankton that no research fleet could provide.

Reductions in marine pollution may yield climate-relevant co-benefits through the protection of biological productivity and may also support ecosystem recovery in a manner complementary to reducing carbon dioxide emissions. The GOES sampler allows these data to be collected, and on that evidence, informed decisions and actions could be taken to protect marine life, nature and public health, and to test whether the condition of the surface microlayer affects evaporation and so has a climate role.

Methods

Sampler and field protocol

The GOES sampler (Fig. 2) is a self-contained cartridge made from a Ø50 mm by 380 mm PVC tube with a slip-over end cap. It houses two acrylic filter plates, each with one central and four Ø5 mm holes on a Ø20 mm pitch circle, inside a standard PVC solvent-weld pipe union. The cartridge hung on stainless steel wire in this survey, and a Kevlar cord is specified for future campaigns. The filter paper is Camlab product 1173270, Grade 4, which is equivalent to Whatman Grade 4 and has a nominal particle retention of 20 to 25 µm. As the cake builds during gravity filtration, smaller particles are also retained. The phytoplankton class describes microphytoplankton and larger colonies, because most cells smaller than 20 µm pass the filter, and pico- and nanophytoplankton supply about 82% of primary production in the North Atlantic gyre[87]. Each fill draws a fixed 0.5-litre sample, independent of vessel speed, and the 500 mL gravity filters go through five Ø5 mm holes onto five sections of filter paper of 5 mm diameter. The sampler was designed by H.D. and manufactured by Calplas.

Crews collected samples at about 12-hour intervals, at 12:00 and 24:00 local time, from the stern or the leeward side of the vessel. They flushed the tube three times with ambient water, dropped it to fill by immersion in the top 250 mm of the water column and capped it as soon as it left the water. The cartridge stayed capped until examination, and after draining for four hours, each plate was opened for

imaging and exposed to air for five minutes or less. Volunteers were told to avoid fleece and other fibre-shedding clothing while sampling. A field guide for volunteers gives the build details and the protocol.

Image acquisition

Filters were photographed on digital microscopes with a 5 mm field of view, a sensor of at least 5 megapixels and a polarising filter. In accepted photographs the fitted 5 mm disc spans a median of 1,456 pixels (range 842 to 1,792), which gives a median pixel pitch of 3.4 µm (range 2.8 to 5.9 µm). A 20 µm object therefore spans about six pixels, and a 300 µm copepod about 90 pixels. Positions came from the image GPS, where the file carries one, and otherwise from the field spreadsheet. Per-image timestamps exist only for the Copepod crossing, and the sampling dates of all vessels fall between 18 December 2021 and 11 February 2022, while the camera date stamps of the Emma return leg run from 19 May to 31 July 2022.

Image curation and analysis

A documented curation stage judged every photograph individually and recorded a decision and a reason for each file. Each accepted photograph shows one 5 mm aperture and represents 0.1 litre of filtered seawater, which is 0.5 litre divided by five holes. Counts were made inside the inner 90% of the disc diameter, which removes edge artefacts and leaves 81% of the disc area, so each photograph counts 0.081 litre. A deterministic pipeline then processed each image: it subtracts the local background, finds the 5 mm filter disc separately in each photograph, and detects and sizes every object larger than 20 µm against that disc. Stated rules for colour, saturation, hue, darkness and elongation assign each object to one of eight classes: phytoplankton, microzooplankton, plastic particle, plastic fibre, dark opaque particle, mineral grain, plant debris or unidentified. We call the plastic particle and plastic fibre classes suspected microplastics because the rules are optical. Size is the diameter of a circle of the same area as the object for every class, fibres included. The rule for dark opaque particles is applied before the 20 µm floor, so 239 of the 6,671 objects in that class (3.6%) have equivalent diameters between 14 and 20 µm. Fibre lengths in Supplementary Table S3 are long-axis measurements, calculated as the minor-axis width multiplied by the elongation. The lead author inspected every object of 250 µm and above by eye. The scripts, the per-image output and the curation list are archived so that the analysis can be rerun end to end (data availability and code availability).

Blind classification check

We tested the classification with three blind marking sheets, which were a pilot sheet of 180 objects, 30 from each of six machine classes, and two clean rounds of 300 objects each, with 50 objects from each of the five major classes and 25 each from the microplastic particle and unidentified classes in each round. The first clean round was marked in two documents of 150 objects each. The pilot sheet used a

ring marker that could hide the edge of an object and was not pooled. Objects were drawn at random and shown to the lead author with the machine class hidden and the order shuffled, and an arrow pointed to each object. Faint rings and halos were ignored as reflection and residual water artefacts. The eye verdicts were scored against the machine classes to give per-class accuracies. For the corrected concentrations, the count in each machine class was divided among the classes assigned by eye in the proportions of the first scorer's verdicts for that machine class in the two clean rounds, and the divided counts were then summed by class. The two clean rounds supply 100 objects for each of the five major classes and 50 each for microplastic particles and unidentified objects, so class accuracy carries an uncertainty of roughly 10 percentage points for the major classes and roughly 14 for the other two. A second scorer (D.D.) then rescored all 780 marked objects blind. Twelve objects lacked a verdict from one scorer and were excluded, which left 768 pairs. We calculated percentage agreement and Cohen's kappa for the seven classes and for collapsed groups of anthropogenic, natural and other objects. We use the scale of Landis and Koch only as a label, because its thresholds are conventional and have been criticised as arbitrary[88,89].

Contamination controls

The sampler is an open system that fills by immersion, like a plankton net, so as with net tows, no procedural blank applies to the deployment, and contamination control rests on the handling protocol. The section on the sampler and field protocol describes the capping of the cartridge, the limit of five minutes in air and the rule on clothing.

Statistical analysis

Presence percentages carry 95% Wilson score intervals, which stay reliable when many photographs hold a zero count for a class. The density of animals in the filtered volume carries an exact 95% Poisson interval. Longitudinal structure was tested for each class by weighted least squares on the logarithm of the mean concentration in 5° longitude bins, weighted by the number of photographs in each bin, with a Spearman rank correlation on individual photographs as a check. Size distributions were fitted as power laws over 20 to 100 µm, where the bin counts are reliable. Agreement between scorers was measured by percentage agreement and by Cohen's kappa, which corrects agreement for chance. All analyses were scripted in Python 3.14, with OpenCV 5.0 and NumPy 2.5 for the image processing, SciPy 1.18 for the statistics and Matplotlib 3.11 for the figures, and the scripts for counting, tables and statistics are archived at Zenodo with the data.

Mineral mass and dust budget

Mineral grains were treated as plates with three tenths of the volume of a sphere of the same projected area. This follows from a measured median long-to-short axis ratio of 1.8, against published medians of

1.70 for length-to-width and 0.40 for height-to-width[90,91], because a grain of those proportions holds 0.31 of the volume of a sphere of the same projected area. Mass was calculated for a mineral density of 2,650 kg m^{-3}, which is the density of quartz. We summed the mass of the 3,881 grains grain by grain across every measured diameter and scaled the sum by the eye-corrected count for the lower estimate. The dust prediction balanced a deposition flux of about 139 million tonnes per year over the 21.2 million km^2 of the deposition corridor[24,25] against the settling velocity of plates, assuming a steady state with no turbulent mixing.

Satellite data

Monthly chlorophyll-a from MODIS-Aqua (product erdMH1chlamday), averaged over January and February 2022, was served by NOAA CoastWatch ERDDAP. Cloud gaps, which cover 5.6% of ocean pixels, were filled from the January to February mean of 2012 to 2021. The median and the share of pixels below 0.15 mg m^{-3} were calculated inside the transect box. Annual mean chlorophyll-a for 5° to 20° N and 20° to 50° W came from the ESA Ocean Colour CCI v6.0 merged record for 1998 to 2025, and the diffuse attenuation coefficient Kd490 came from the merged record and from MODIS-Aqua R2018.0 for 2003 to 2021. These records were served by the Plymouth Marine Laboratory THREDDS server and the NOAA OceanWatch ERDDAP server. Of the merged ocean colour products, OC-CCI gives the most conservative estimates of long-term change, because it applies a common atmospheric correction and an inter-sensor bias correction before merging[31]. Least squares fits give slopes and p-values corrected for first-order autocorrelation. Attenuation in excess of chlorophyll was tested as the trend in the residuals of a regression of the logarithm of annual Kd490 on the logarithm of annual chlorophyll-a.

Use of generative AI

A generative AI system (Anthropic's Claude) was used under the authors' direction for the image-analysis pipeline code, the curation and eye-check statistics, the inter-scorer agreement calculation, the longitudinal regressions, figure generation, literature checks and copy editing. All data, interpretations and conclusions are the authors' own, the authors reviewed and verified every output, and they take full responsibility for the content. No text, figure or data in this paper was generated by AI without that review, and no AI-generated images are used.

Declarations

Data availability

The complete data set underlying this study is openly archived in the Zenodo repository (https://doi.org/10.5281/zenodo.21477681). It comprises the per-station particle counts, the individual particle-size measurements, the per-image census, the frame-curation list with a stated reason for every excluded file, the station-level table and the crew field logs. The crew handlogs are provided as

qualitative context only and are not used in the quantitative analysis, which rests on the deposited image pipeline. The volunteer field guide describing the sampler build and the protocol is available at https://goesfoundation.com/water-sampling-field-guide-for-volunteers/, and an archived copy is in the same Zenodo record. The MODIS-Aqua monthly chlorophyll-a product (erdMH1chlamday) is available from NASA Ocean Colour and from the NOAA CoastWatch ERDDAP server. The ESA Ocean Colour CCI v6.0 chlorophyll-a and Kd490 records are served by the Plymouth Marine Laboratory THREDDS server, and the MODIS-Aqua Kd490 R2018.0 record by the NOAA OceanWatch ERDDAP server.

Code availability

The code that sizes and classifies the objects, recomputes the tables and statistics and applies the eye-check correction is archived in the same Zenodo record (https://doi.org/10.5281/zenodo.21477681), together with the satellite series analysed in the paper. The particle-classification image pipeline, including the frame-curation stage and the detection, sizing, classification and aggregation scripts with their complete per-image output, is deposited in the same record, so the analysis can be reproduced end to end from the archived images.

Acknowledgements

We thank the volunteer skippers and crews of the participating vessels (Copepod, Emma, Misty Blue, Eleuthera, Yolo, Ya, Jiyu, Imagine, Meander, Elixir, Thetis, Sunflower and Ari), without whom this survey would not have been possible. We thank the Viking Explorers yacht rally (www.vikingexplorersrally.com) for allowing us to work with their clients to recruit the survey yachts. We thank Calplas (Basque Country, Spain) for manufacturing the sampling filter. This research received no specific grant from any public, commercial or not-for-profit funding agency. Volunteer crews conducted the fieldwork, with support from the GOES Foundation.

Author contributions

H.D. conceived and led the GOES project, designed the sampling protocol, and led the analysis and writing. D.D. contributed to the study design and to the manuscript and served as the second scorer for the blind classification check. H.D. and D.D. skippered the sailing vessel Copepod, which provided the GPS-tagged reference crossing. The participating vessel crews collected the remaining field samples and microscope images. Both authors reviewed the manuscript in full and approved the final version for submission.

Competing interests

The authors are associated with the GOES Foundation, a not-for-profit organisation originally based on the sailing vessel Copepod and now located at www.seahorsepoint.org in Bocas del Toro, Panama, and H.D. designed the GOES filter that this paper evaluates. The authors declare that they have no financial competing interests.

References

1. de Fernández ML et al (2019) Zooplankton abundance and diversity in the tropical and subtropical ocean. Diversity 11:203
2. Mériguet Z et al (2025) Quantitative imaging datasets of surface micro- to mesoplankton communities and microplastic across the Pacific and North Atlantic oceans from the Tara Pacific expedition. Earth Syst Sci Data 17:2761–2792
3. Geyer R, Jambeck JR, Law KL (2017) Production, use, and fate of all plastics ever made. Sci Adv 3:e1700782
4. Kooi M, van Nes EH, Scheffer M, Koelmans AA (2017) Ups and downs in the ocean: effects of biofouling on vertical transport of microplastics. Environ Sci Technol 51:7963–7971
5. Erni-Cassola G, Zadjelovic V, Gibson MI, Christie-Oleza JA (2019) Distribution of plastic polymer types in the marine environment: a meta-analysis. J Hazard Mater 369:691–698
6. Kukulka T, Proskurowski G, Morét-Ferguson S, Meyer DW, Law KL (2012) The effect of wind mixing on the vertical distribution of buoyant plastic debris. Geophys Res Lett 39:L07601
7. Reisser J et al (2015) The vertical distribution of buoyant plastics at sea: an observational study in the North Atlantic Gyre. *Biogeosciences*12, 1249–1256
8. Jickells TD et al (2005) Global iron connections between desert dust, ocean biogeochemistry, and climate. Science 308:67–71
9. Mills MM, Ridame C, Davey M, La Roche J, Geider RJ (2004) Iron and phosphorus co-limit nitrogen fixation in the eastern tropical North Atlantic. Nature 429:292–294
10. Moore CM et al (2013) Processes and patterns of oceanic nutrient limitation. Nat Geosci 6:701–710
11. Goldenberg SB, Shapiro LJ (1996) Physical mechanisms for the association of El Niño and West African rainfall with Atlantic major hurricane activity. J Clim 9:1169–1187
12. Cunliffe M et al (2013) Sea surface microlayers: a unified physicochemical and biological perspective. Prog Oceanogr 109:104–116
13. Trenberth KE, Smith L, Qian T, Dai A, Fasullo J (2007) Estimates of the Global Water Budget and Its Annual Cycle Using Observational and Model Data. J Hydrometeorol 8:758–769
14. Pereira R, Ashton I, Sabbaghzadeh B, Shutler JD, Upstill-Goddard RC (2018) Reduced air–sea CO_2 exchange in the Atlantic Ocean due to biological surfactants. Nat Geosci 11:492–496
15. Mustaffa NIH, Ribas-Ribas M, Banko-Kubis HM, Wurl O (2020) Global reduction of in situ CO_2 transfer velocity by natural surfactants in the sea-surface microlayer. *Proc. R. Soc. A*476, 20190763
16. Wurl O et al (2018) Warming and inhibition of salinization at the ocean's surface by cyanobacteria. Geophys Res Lett 45:4230–4237
17. Trenberth KE, Caron JM (2001) Estimates of meridional atmosphere and ocean heat transports. J Clim 14:3433–3443

18. Johns WE et al (2011) Continuous, array-based estimates of Atlantic Ocean heat transport at 26.5° N. J Clim 24:2429–2449
19. Wurl O, Ekau W, Landing WM, Zappa CJ (2017) Sea surface microlayer in a changing ocean, a perspective. Elem Sci Anth 5:31
20. Aiken J et al (2000) The Atlantic Meridional Transect: overview and synthesis of data. Prog Oceanogr 45:257–312
21. Boltovskoy D, Kling SA, Takahashi K, Bjørklund K (2010) World atlas of distribution of recent Polycystina (Radiolaria). Palaeontol Electron 13, 13.3.18A
22. Tréguer P, De La Rocha CL (2013) The World Ocean Silica Cycle. Annu Rev Mar Sci 5:477–501
23. Mériguet Z et al (2024) Global scale surface meso-plankton dataset collected with High-Speed Net and imaged with ZooScan during the Tara Pacific Expedition. SEANOE https://doi.org/10.17882/102336
24. Yu H et al (2015) Quantification of trans-Atlantic dust transport from seven-year (2007–2013) record of CALIPSO lidar measurements. Remote Sens Environ 159:232–249
25. Kaufman YJ et al (2005) Dust transport and deposition observed from the Terra-Moderate Resolution Imaging Spectroradiometer (MODIS) spacecraft over the Atlantic Ocean. J Geophys Res 110, D10S12
26. Franz BA, Cetinić I, Gao M, Westberry TK (2026) Global ocean phytoplankton. In State of the Climate in 2025 (eds Volkov, D. L. & Perez, R. C.) Bull. Am. Meteorol. Soc. 107, S207–S211. https://doi.org/10.1175/BAMS-D-26-0100.1
27. Cael BB, Bisson K, Boss E, Dutkiewicz S, Henson S (2023) Global climate-change trends detected in indicators of ocean ecology. Nature 619:551–554
28. Dutkiewicz S et al (2019) Ocean colour signature of climate change. Nat Commun 10:578
29. Jenkinson IR (1986) Oceanographic implications of non-Newtonian properties found in phytoplankton cultures. Nature 323:435–437
30. Passow U (2002) Transparent exopolymer particles (TEP) in aquatic environments. Prog Oceanogr 55:287–333
31. Cheatham S, Koestner D, Hamre B (2026) The ocean's color is changing near the Great Pacific Garbage Patch. Commun Earth Environ 7:855
32. Pabortsava K, Lampitt RS (2020) High concentrations of plastic hidden beneath the surface of the Atlantic Ocean. Nat Commun 11:4073
33. ten Hietbrink S, Materić D, Holzinger R, Groeskamp S, Niemann H (2025) Nanoplastic concentrations across the North Atlantic. Nature 643:412–416
34. Stead JL et al (2020) Identification of tidal trapping of microplastics in a temperate salt marsh system using sea surface microlayer sampling. Sci Rep 10:14147
35. Löder MGJ, Gerdts G (2015) In: Marine Anthropogenic L, Bergmann M, Gutow L, Klages M (eds) Methodology used for the detection and identification of microplastics: a critical appraisal. Springer,

pp 201–227

36. Prata JC, da Costa JP, Duarte AC, Rocha-Santos T (2019) Methods for sampling and detection of microplastics in water and sediment: a critical review. TrAC Trends Anal Chem 110:150–159
37. Allen S et al (2019) Atmospheric transport and deposition of microplastics in a remote mountain catchment. Nat Geosci 12:339–344
38. Brahney J et al (2021) Constraining the atmospheric limb of the plastic cycle. *Proc. Natl Acad. Sci. USA*118, e2020719118
39. van der Does M et al (2019) Tropical rains controlling deposition of Saharan dust across the North Atlantic Ocean. *Geophys. Res. Lett.*47, eGL086867 (2020)
40. China S et al (2015) Morphology and mixing state of aged soot particles at a remote marine free troposphere site: implications for optical properties. Geophys Res Lett 42:1243–1250
41. Han YM, Cao J, Lee SC, Ho KF, An ZS (2010) Different characteristics of char and soot in the atmosphere and their ratio as an indicator for source identification in Xi'an, China. Atmos Chem Phys 10:595–607
42. Gilgen A et al (2018) Implementing microscopic charcoal particles into a global aerosol–climate model. Atmos Chem Phys 18:11813–11829
43. Swindles GT et al (2015) Spheroidal carbonaceous particles are a defining stratigraphic marker for the Anthropocene. Sci Rep 5:10264
44. Kovochich M et al (2021) Chemical mapping of tire and road wear particles for single particle analysis. Sci Total Environ 757:144085
45. Evangeliou N et al (2020) Atmospheric transport is a major pathway of microplastics to remote regions. Nat Commun 11:3381
46. Dittmar S et al (2025) Settling velocities of tire and road wear particles: analysing finely graded density fractions of samples from a road simulator and a highway tunnel. Environ Sci Technol 59:13434–13446
47. Gao Z et al (2022) On airborne tire wear particles along roads with different traffic characteristics using passive sampling and optical microscopy, single particle SEM/EDX, and μ-ATR-FTIR analyses. Front Environ Sci 10:1022697
48. Cornelissen G et al (2005) Extensive sorption of organic compounds to black carbon, coal, and kerogen in sediments and soils: mechanisms and consequences for distribution, bioaccumulation, and biodegradation. Environ Sci Technol 39:6881–6895
49. Mato Y et al (2001) Plastic resin pellets as a transport medium for toxic chemicals in the marine environment. Environ Sci Technol 35:318–324
50. Beckingham B, Ghosh U (2017) Differential bioavailability of polychlorinated biphenyls associated with environmental particles: microplastic in comparison to wood, coal and biochar. Environ Pollut 220:150–158

51. Koelmans AA, Bakir A, Burton GA, Janssen CR (2016) Microplastic as a vector for chemicals in the aquatic environment: critical review and model-supported reinterpretation of empirical studies. Environ Sci Technol 50:3315–3326
52. Katsoyiannis A, Samara C (2004) Persistent organic pollutants (POPs) in the sewage treatment plant of Thessaloniki, northern Greece: occurrence and removal. Water Res 38:2685–2698
53. Arvaniti OS, Stasinakis AS (2015) Review on the occurrence, fate and removal of perfluorinated compounds during wastewater treatment. Sci Total Environ 524–525:81–92
54. Kelessidis A, Stasinakis AS (2012) Comparative study of the methods used for treatment and final disposal of sewage sludge in European countries. Waste Manage 32:1186–1195
55. Pozzebon EA, Seifert L (2023) Emerging environmental health risks associated with the land application of biosolids: a scoping review. Environ Health 22:57
56. Blaine AC et al (2013) Uptake of perfluoroalkyl acids into edible crops via land applied biosolids: field and greenhouse studies. Environ Sci Technol 47:14062–14069
57. Lindstrom AB et al (2011) Application of WWTP biosolids and resulting perfluorinated compound contamination of surface and well water in Decatur, Alabama, USA. Environ Sci Technol 45:8015–8021
58. Duce RA et al (1991) The atmospheric input of trace species to the world ocean. Global Biogeochem Cy 5:193–259
59. Jurado E et al (2004) Atmospheric dry deposition of persistent organic pollutants to the Atlantic and inferences for the global oceans. Environ Sci Technol 38:5505–5513
60. Wurl O, Obbard JP (2004) A review of pollutants in the sea-surface microlayer (SML): a unique habitat for marine organisms. Mar Pollut Bull 48:1016–1030
61. Ziccardi L, Edgington A, Hentz K, Kulacki K, Driscoll S (2016) Microplastics as vectors for bioaccumulation of hydrophobic organic chemicals in the marine environment: a state-of-the-science review. Environ Toxicol Chem 35:1667–1676
62. Rubin AE, Zucker I (2022) Interactions of microplastics and organic compounds in aquatic environments: a case study of augmented joint toxicity. Chemosphere 289:133212
63. O'Dowd CD et al (2004) Biogenically driven organic contribution to marine aerosol. Nature 431:676–680
64. Pérez V, Fernández E, Marañón E, Morán XAG, Zubkov MV (2006) Vertical distribution of phytoplankton biomass, production and growth in the Atlantic subtropical gyres. Deep-Sea Res Pt I 53:1616–1634
65. Cornec M et al (2020) Deep chlorophyll maxima in the global ocean: occurrences, drivers and characteristics. *Global Biogeochem. Cy.*35, eGB006759 (2021)
66. Johnsen S, Widder EA (2001) Ultraviolet absorption in transparent zooplankton and its implications for depth distribution and visual predation. Mar Biol 138:717–730

67. Tedetti M, Sempéré R (2006) Penetration of ultraviolet radiation in the marine environment. A review. Photochem Photobiol 82:389–397
68. Al-Aidaroos AM et al (2015) Strong sensitivity of Red Sea zooplankton to UV-B radiation. Estuaries Coasts 38:846–853
69. Duan J, Gregory J (2003) Coagulation by hydrolysing metal salts. Adv Colloid Interface Sci 100–102:475–502
70. Louis J, Pedrotti ML, Gazeau F, Guieu C (2017) Experimental evidence of formation of transparent exopolymer particles (TEP) and POC export provoked by dust addition under current and high pCO_2 conditions. PLoS ONE 12:e0171980
71. Seuront L, Vincent D, Mitchell JG (2006) Biologically induced modification of seawater viscosity in the Eastern English Channel during a *Phaeocystis globosa* spring bloom. J Mar Syst 61:118–133
72. Larsen PS, Riisgård HU (2009) Viscosity and not biological mechanisms often controls the effects of temperature on ciliary activity and swimming velocity of small aquatic organisms. J Exp Mar Biol Ecol 381:67–73
73. Li C et al (2026) Aging transforms marine microplastics into reactive interfaces with environmental consequences. iScience 29:116102
74. Desforges J-PW, Galbraith M, Ross PS (2015) Ingestion of microplastics by zooplankton in the NE Pacific. Arch Environ Contam Toxicol 69:320–330
75. Ma H et al (2020) Microplastics in aquatic environments: toxicity to trigger ecological consequences. Environ Pollut 261:114089
76. Cole M, Lindeque P, Fileman E, Halsband C, Galloway TS (2015) The impact of polystyrene microplastics on feeding, function and fecundity in the marine copepod *Calanus helgolandicus*. Environ Sci Technol 49:1130–1137
77. Sjollema SB, Redondo-Hasselerharm P, Leslie HA, Kraak MHS, Vethaak A (2016) D. Do plastic particles affect microalgal photosynthesis and growth? Aquat Toxicol 170:259–261
78. Tetu SG et al (2019) Plastic leachates impair growth and oxygen production in *Prochlorococcus*, the ocean's most abundant photosynthetic bacteria. Commun Biol 2:184
79. Na J, Song J, Achar JC, Jung J (2021) Synergistic effect of microplastic fragments and benzophenone-3 additives on lethal and sublethal *Daphnia magna* toxicity. J Hazard Mater 402:123845
80. Polidoro B, Lewis T, Clement C (2022) A screening-level human health risk assessment for microplastics and organic contaminants in near-shore marine environments in American Samoa. Heliyon 8:e09101
81. Gewert B, MacLeod M, Breitholtz M (2021) Variability in toxicity of plastic leachates as a function of weathering and polymer type: a screening study with the copepod Nitocra spinipes. Biol Bull 240:191–199

82. Simon M, Hartmann NB, Vollertsen J (2021) Accelerated weathering increases the release of toxic leachates from microplastic particles as demonstrated through altered toxicity to the green algae *Raphidocelis subcapitata*. Toxics 9:185
83. Nguyen TT, Park K, Kim S, Kwak I-S (2026) Toxicity of nano- and microplastics on marine and freshwater fish: a multi-scale perspective from organ systems to cells. Water Biol Secur 5:100534
84. Žutić V, Ćosović B, Marčenko E, Bihari N, Kršinić F (1981) Surfactant production by marine phytoplankton. Mar Chem 10:505–520
85. Kujawinski EB, Farrington JW, Moffett JW (2002) Evidence for grazing-mediated production of dissolved surface-active material by marine protists. Mar Chem 77:133–142
86. Wurl O, Wurl E, Miller L, Johnson K, Vagle S (2011) Formation and global distribution of sea-surface microlayers. Biogeosciences 8:121–135
87. Tilstone GH, Lange PK, Misra A, Brewin RJW, Cain T (2017) Micro-phytoplankton photosynthesis, primary production and potential export production in the Atlantic Ocean. Prog Oceanogr 158:109–129
88. Landis JR, Koch GG (1977) The measurement of observer agreement for categorical data. Biometrics 33:159–174
89. Feinstein AR, Cicchetti DV (1990) High agreement but low kappa: I. The problems of two paradoxes. J Clin Epidemiol 43:543–549
90. Huang Y, Kok JF, Saito M, Muñoz O (2023) Single-scattering properties of ellipsoidal dust aerosols constrained by measured dust shape distributions. Atmos Chem Phys 23:2557–2577
91. Kandler K et al (2011) Electron microscopy of particles collected at Praia, Cape Verde, during the Saharan Mineral Dust Experiment: particle chemistry, shape, mixing state and complex refractive index. Tellus B 63:475–496

Figures

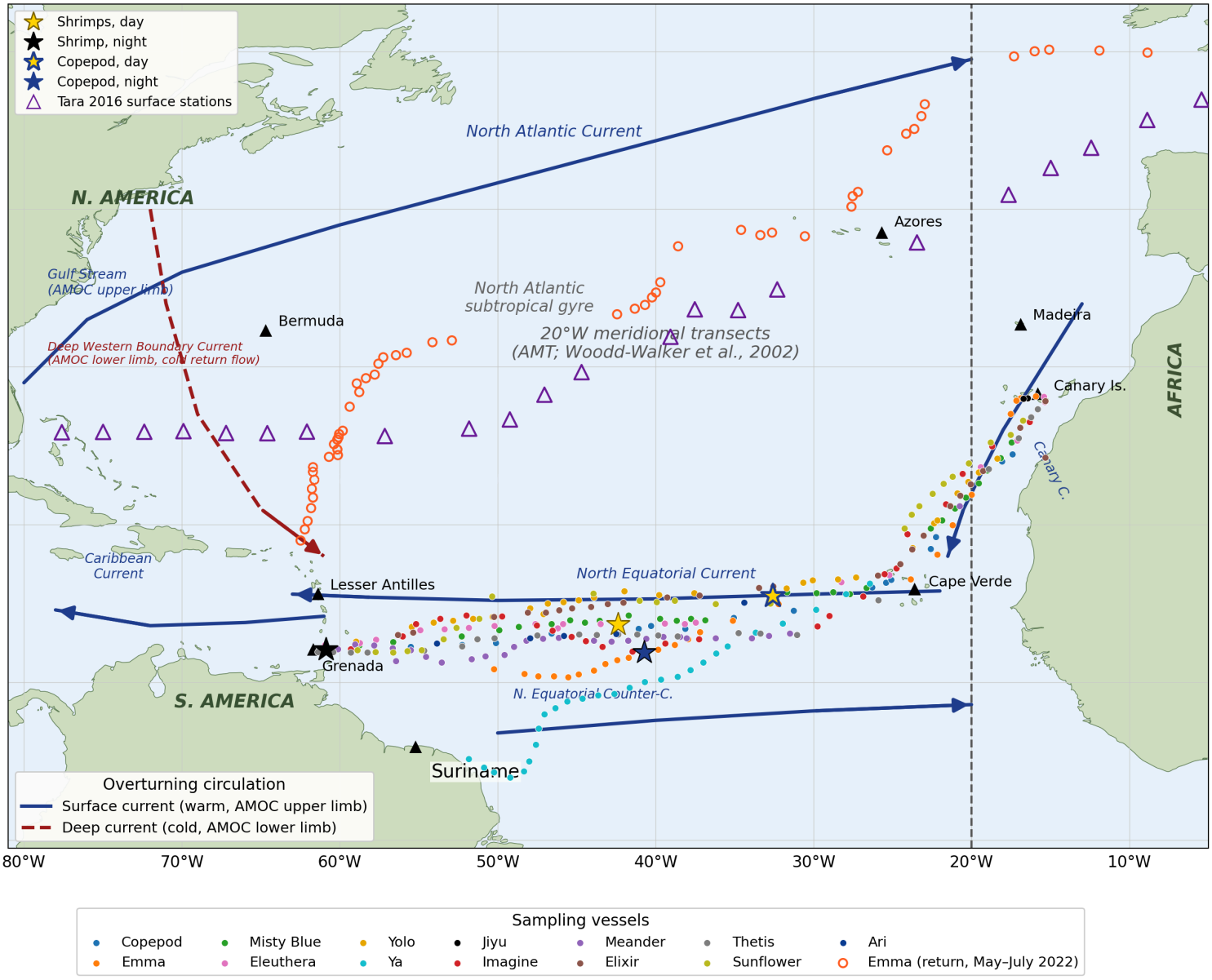


Figure 1

Study region and sampling stations of the thirteen yachts that crossed the trade wind in the North Atlantic. The yachts sailed from the Canary Islands and Cape Verde to Grenada and Suriname between 18 December 2021 and 11 February 2022, and the yacht Emma also sailed a higher-latitude return leg between 19 May and 31 July 2022 (open orange circles). Filled circles are stations of the crossing, coloured by vessel. Stars mark the four stations where animals were found, with yellow for daytime samples and black or blue for night samples, so that the five animals appear as four stars. Open purple triangles mark the twenty-two surface stations of the 2016 Tara Pacific crossing within the map area, and the dashed line at 20° W marks the corridor of the Atlantic Meridional Transect. Blue arrows show surface currents, and the dashed red line shows the deep western boundary current, both drawn schematically for orientation, and the coastlines are © Natural Earth.

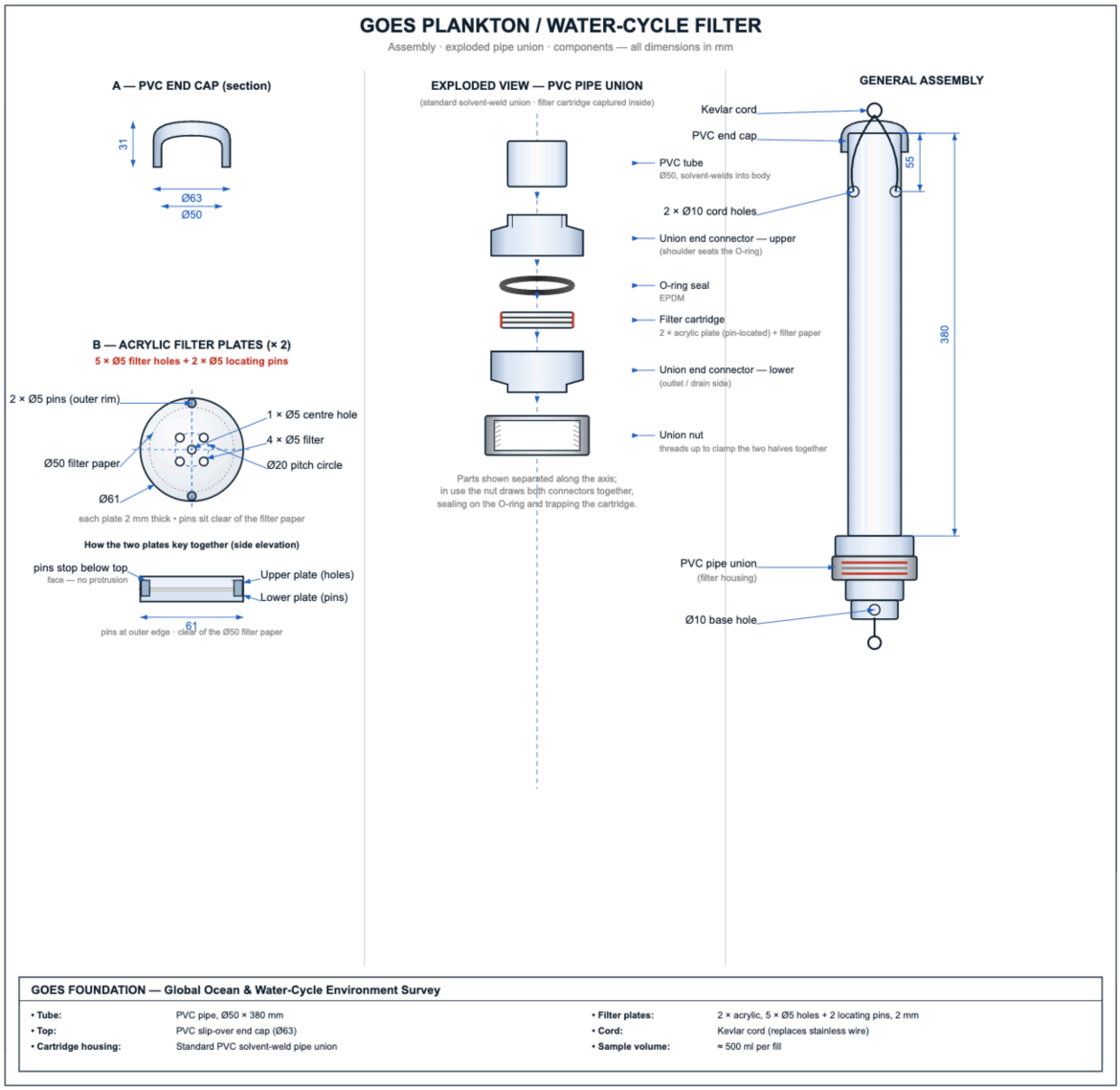


Figure 2

The GOES sampler is shown as an assembled cartridge and as its separate parts. The panels show the PVC end cap, the two acrylic filter plates with five Ø5 mm filter holes and two locating pins, the exploded view of the PVC pipe union with its filter cartridge, and the general assembly. The Ø50 mm tube mouth admits the 0.5-litre sample, which then gravity-filters through the five Ø5 mm apertures of the two plates that sandwich a filter paper of 20 µm nominal retention. The cartridge draws a fixed 0.5-litre sample independent of the speed of the vessel and, suspended on its line, filters vertically while the boat moves.

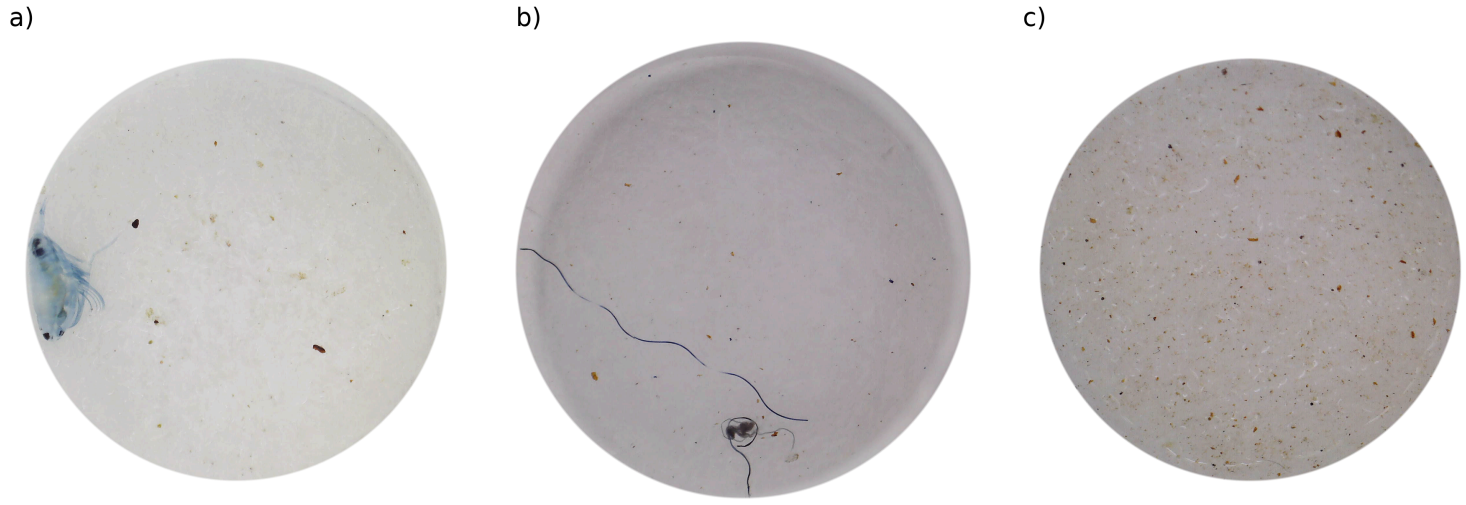
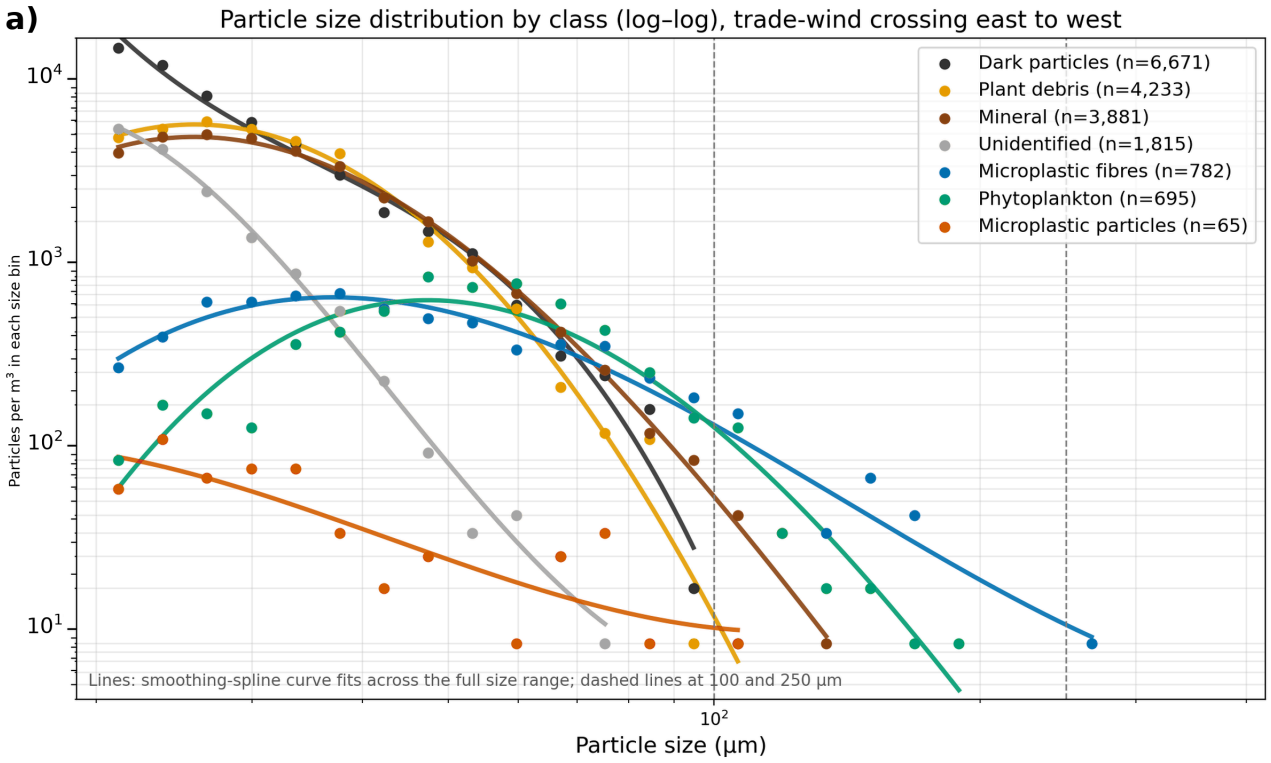


Figure 3

Representative filter fields from three different stations of the survey. Each panel is a separate 0.5-litre sample and not a different hole of the same filter, and each field shows the particle content of about 100 mL of seawater. The faint grey circle marks the 5 mm field boundary. a) One of the two blue copepods. b) A single long blue microplastic fibre, several millimetres long, and a black fibre coil. c) Brown mineral grains together with dark opaque particles. All identifications in these panels are optical and await confirmation by spectroscopy.



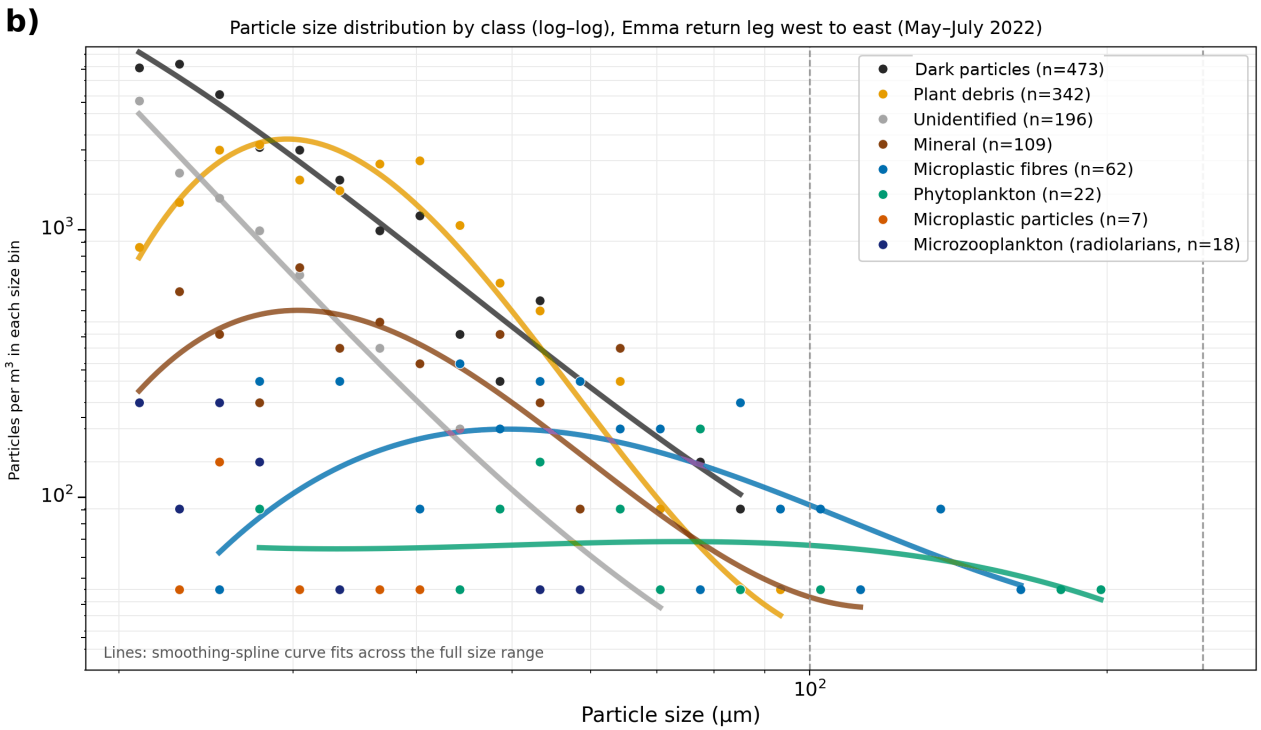


Figure 4

Smoothed size distribution of each particle class on logarithmic axes for a) the trade-wind crossing (18,142 objects) and b) the Emma return leg (1,229 objects). Points give the concentration in each size bin, in particles per cubic metre of the counted volume (118.7 litres in a and 22.0 litres in b), and lines are smoothing-spline fits across the full size range. Dashed lines mark 100 µm and 250 µm, fibres are plotted by equivalent circular diameter like every other class, and their lengths are given in

Supplementary Table S3. The power-law exponents in the text are fitted over 20 to 100 µm only; the two counted copepods are not shown, and the radiolarian class appears in panel b only.

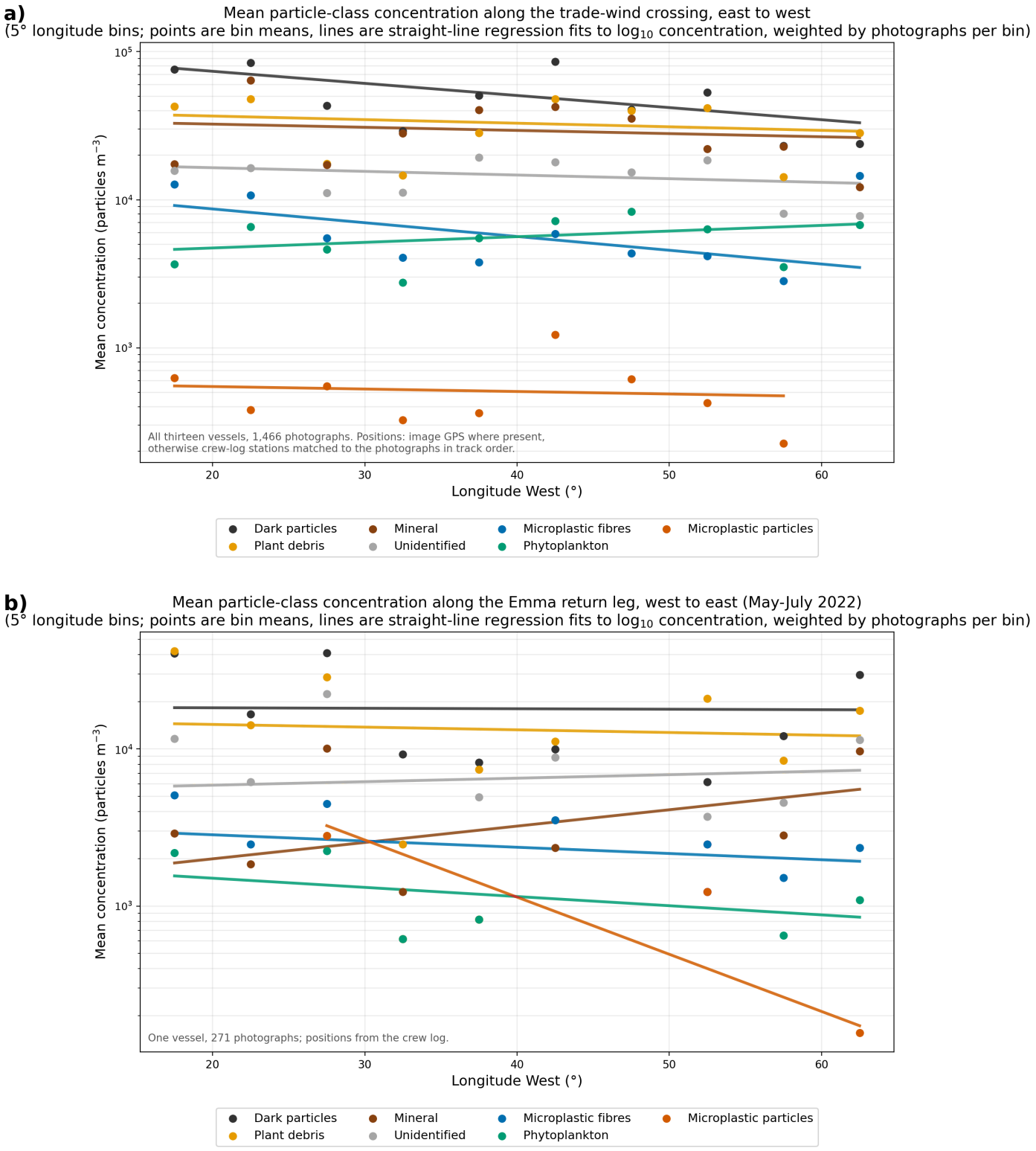


Figure 5

Mean particle-class concentration in 5° longitude bins for the crossing and the return leg. a) The trade wind crossing from east to west, with all thirteen vessels contributing (1,466 photographs). b) The Emma

return leg from west to east (one vessel, 271 photographs). Points are bin means, and lines are straight-line fits to the logarithm of concentration against longitude, weighted by the number of photographs in each bin. Positions are per-image GPS, where the file carries one, and otherwise the crew-log stations are matched to the photographs in track order. No fitted slope is significant at the 5% level, and zooplankton is too scarce to plot. The classes are the machine classes before the eye-check correction, and they are optical classes pending spectroscopic confirmation.

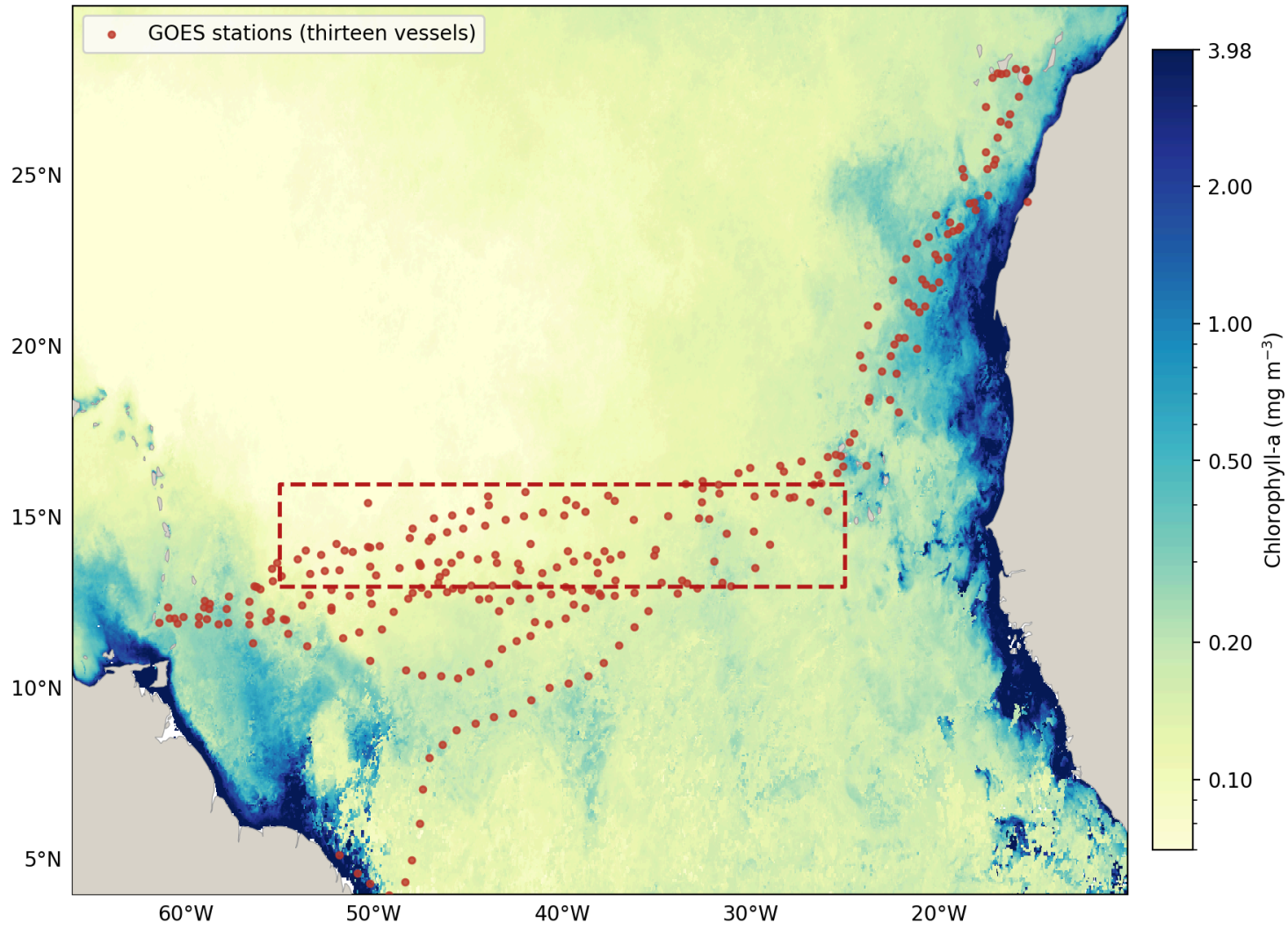


Figure 6

Satellite chlorophyll-a over the study region in January and February 2022, with the GOES stations. The map shows the MODIS-Aqua monthly product on a logarithmic colour scale, with the GOES sampling stations in red and the trade-wind transect box as a dashed line. Cloud gaps, which cover 5.6% of ocean pixels, were filled from the January to February mean of 2012 to 2021. The crossing runs through oligotrophic water on the southern flank of the subtropical gyre, and elevated chlorophyll is restricted to the Mauritanian and equatorial upwellings and the continental margins. Chlorophyll-a data © NASA Ocean Biology Processing Group (MODIS-Aqua), served by NOAA CoastWatch ERDDAP, and the coastlines are © Natural Earth.

Supplementary Files

This is a list of supplementary files associated with this preprint. Click to download.

- 3SupplementaryInformation.docx